

# Theoretical analysis for dynamic contact angle hysteresis on chemically patterned surfaces

Xianmin Xu\*

*LSEC,ICMSEC, NCMIS, Academy of Mathematics and Systems Science,  
Chinese Academy of Sciences, Beijing 100190, China*

Xiaoping Wang†

*Department of Mathematics, Hong Kong University of Science and Technology,  
Clear Water Bay, Kowloon, Hong Kong, China*

## Abstract

A dynamic wetting problem is studied for a moving thin fiber inserted in fluid and with a chemically inhomogeneous surface. A reduced model is derived for contact angle hysteresis by using the Onsager principle as an approximation tool. The model is simple and captures the essential dynamics of the contact angle. From this model we derive an upper bound of the advancing contact angle and a lower bound of the receding angle, which are verified by numerical simulations. The results are consistent with the quasi-static results. The model can also be used to understand the asymmetric dependence of the advancing and receding contact angles on the fiber velocity, which is observed recently in physical experiments reported in *Guan et al Phys. Rev. Lett. 2016*.

---

\* Corresponding author, xmxu@lsec.cc.ac.cn

† mawang@ust.hk

## I. INTRODUCTION

Wetting is a common phenomenon in nature and our daily life. It is a fundamental problem with applications in many industrial processes, like coating, printing and oil industry, etc. In equilibrium state, wetting on smooth homogeneous surfaces can be described by the Young's equation [1]. It becomes much more complicated when the solid surface is geometrically rough or chemically homogeneous [2–6]. The apparent contact angle on rough surface is not unique even in equilibrium state. The largest contact angle is called the advancing angle and the smallest is called the receding angle. The difference between them is called contact angle hysteresis (CAH).

Theoretical study on the CAH is difficult due to its multiscale nature. The macroscopic contact angles is affected by the microscopic roughness of the surface. Previous studies mainly focus on quasi-static wetting problems on surface with simple geometry or chemical inhomogeneity (see [7–14] among many others). For example, Joanny and De Gennes analysed the CAH on a surface with dilute defects [8]. Recently, Hatipogullari *et al* studied the CAH in a two dimensional chemically heterogeneous microchannel [14]. Similar problems have also been analysed in [13]. For three dimensional wetting problems on surfaces with periodic roughness, there are only a few results. CAH is partly interpreted using the modified Wenzel and Cassie equations which are derived to describe the meta-stable states on rough surfaces [15–18].

The understanding of CAH in the dynamic wetting problems is still very poor, although there are some interesting observations in experiments[19, 20] and molecular dynamics simulations [21]. One reason is due to the poor understanding of the moving contact line problem. Both modelling and simulations of moving contact line (MCL) problems are challenging in continuum fluid mechanics due to the inherently multiscale nature of MCL [22–30]. When the solid surface is rough or chemically inhomogeneous, there are only a few numerical studies (e.g. [31, 32]) and theoretical analysis [33] on the dynamic wetting problems.

Recently, a powerful approximation tool is developed by using the Onsager variational principle[34, 35]. The main idea is to use the Onsager principle to derive a reduced model for a set of slow variables. The reduced model is much simpler than the original PDE model and it captures the essential dynamics of the slow variables. The method has been applied successfully in many complicated problems in soft matter and also in hydrodynamics[36–

45]. The Onsager principle is capable to describe the moving contact line problem when the capillary number is small and the inertial effect can be ignored. Actually the generalized Navier slip boundary condition for contact line motion was derived by using the Onsager principle [46].

In the paper, we use the Onsager principle as an approximation tool to study the dynamic wetting problem on chemically inhomogeneous surface. We consider the contact line motion on the surface of a thin fiber inserted in fluid. We derive a reduced model consists of two ODEs for the dynamics of the contact angle and position of the contact line by using the Onsager principle. The model is easy to analyse and also easy to solve numerically. Using the model, we derive an upper bound for the advancing angle and a lower bound of the receding angle. Numerical results show that the model can capture the essential features of the dynamic CAH.

We show that the reduced model characterizes nicely the asymmetric dependence of the advancing and receding contact angles on the fiber velocity. The interesting phenomenon has been observed in the recent experiments [20]. It has been partly analysed by using a phase-field model in [47, 48], which is a quasi-static model in which the viscous dissipation of the fluid is ignored. The previous analysis shows that the asymmetric distribution of the chemical inhomogeneity on the solid surface may induce the asymmetric dependence of the advancing and receding contact angles on the velocity. Our analysis in this paper reveals that the asymmetric dependence can also be caused by dynamic effects, since the receding contact angle is more sensitive to the fiber velocity than the advancing angle.

The main structure of the paper is as follows. In section 2, we describe the main idea of using Onsager principle as an approximation tool in free boundary problems. In section 3, we use the method to derive a reduced model for the dynamic wetting problem. In section 4, we show some numerical examples that demonstrate that the model captures the behavior of the contact line motion and CAH nicely. In section 5, we give a few conclusion remarks.

## II. THE ONSAGER PRINCIPLE AS AN APPROXIMATION TOOL

The Onsager principle is a variational principle proposed by Lars Onsager in his celebrated papers on the reciprocal relation[34, 35]. It has been widely used to derive the time evolving equations in soft matter physics[49, 50], such as the Ericksen-Leslie equation in

liquid crystals[51] and the gel dynamics equations[52] among many others. In fluid dynamics, it has also been used to derive a generalized Navier Slip boundary condition for moving contact line problems[46].

Recently, the Onsager principle has also been used as a powerful tool to solve approximately many problems in fluid and soft matter systems [36, 39, 41, 44]. In particular, some free boundary problems in Stokesian hydrodynamics can be solved efficiently by the method [38, 40]. The key idea is described as follows. Suppose we are considering a Stokesian hydrodynamic system which includes some free interfaces (interfaces between fluid and solid or fluid and fluid). The interfaces are moving driven by certain potential forces (gravity, surface tension, etc). Suppose that we are interested only in the time evolution of the free interfaces. Let  $a(t) = \{a_1(t), a_2(t), \dots, a_N(t)\}$  be the set of the parameters which specify the position of the boundaries. By ignoring the inertial effect, the evolution of the system is determined approximately by using the Onsager principle for the parameter set  $a(t)$ . The time derivative  $\dot{a}(t) = \{\dot{a}_1(t), \dot{a}_2(t), \dots, \dot{a}_N(t)\}$  is determined by minimizing the total Rayleighian, which is a function of  $\dot{a}$

$$R(\dot{a}, a) = \Phi(\dot{a}, a) + \sum_i \frac{\partial A}{\partial a_i} \dot{a}_i, \quad (1)$$

where  $A(a)$  is the potential energy of the system, and  $\Phi(\dot{a}, a)$  is the energy dissipation function which is defined as the half of the minimum of the energy dissipated per unit time in the fluid when the boundary is changing at rate  $\dot{a}$ . Since the fluid obeys Stokesian dynamics,  $\Phi(\dot{a}, a)$  is always written as a quadratic function of  $\dot{a}$ .

$$\Phi(\dot{a}, a) = \frac{1}{2} \sum_{i,j} \zeta_{ij}(a) \dot{a}_i \dot{a}_j. \quad (2)$$

The minimum condition of eq.(1)

$$\frac{\partial \Phi}{\partial \dot{a}_i} + \frac{\partial A}{\partial a_i} = 0 \quad \text{or} \quad \sum_j \zeta_{ij}(a) \dot{a}_j = -\frac{\partial A}{\partial a_i}, \quad (3)$$

represents the force balance of two kinds of forces, the hydrodynamic frictional force  $\partial \Phi / \partial \dot{a}_i$ , and the potential force  $-\partial A / \partial a_i$  in the generalized coordinate. The equation (3) gives the dynamics of the parameters  $a(t)$ .

The main feature of the above approach is that the parameter set  $a = \{a_i\}$  may not be a full space to describe the system. It includes only a few slow variables we are interested in. If  $a(t)$  are parameters depending only on time, we are led to a system of ordinary differential equations, which is much easier to solve and analyse than the standard hydrodynamic

equations. In the following, we will use the idea to study the dynamic CAH problem on chemically inhomogeneous surfaces.

### III. THE ANALYSIS OF A DYNAMIC WETTING PROBLEM

Motivated by the recent physical experiments in [20], we consider a dynamic wetting problem as shown in Figure 1. A thin fiber with chemically inhomogeneous surface is inserted in a liquid reservoir. The liquid-air interface forms a circular contact line on the fiber surface. By moving the fiber up and down through the interface with a constant velocity  $v$ , the contact line moves along the surface. When the fiber moves down, the contact line will advance to the upper dry part of the fiber surface. This corresponds to an advancing contact angle. Otherwise, if the fiber moves up, this corresponds to a receding contact angle. We are interested in the dynamic contact angle hysteresis in the process. In particular, how the advancing and receding contact angles change with different velocity  $v$ .

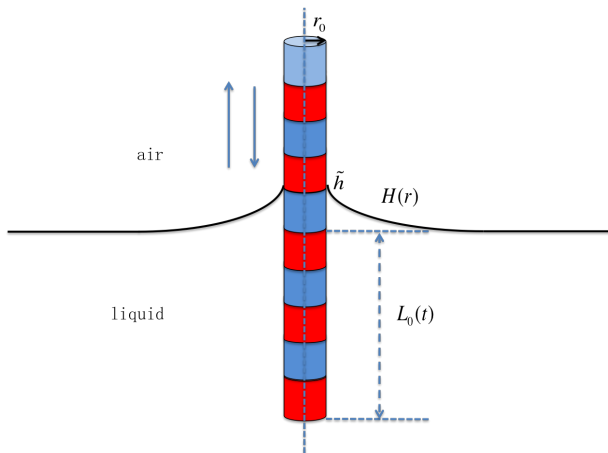


FIG. 1. Fiber with chemically patterned surface in a liquid

To approximate the dynamic wetting problem described above by the Onsager principle, we make some ansatz for the system. At time  $t$ , we assume the liquid-air interface is radial-symmetric and described approximately by the function:

$$z = H(r) := h(t) - r_0 \cos \theta(t) \ln \left( \frac{r + \sqrt{r^2 - r_0^2 \cos^2 \theta(t)}}{r_0 \cos \theta(t)} \right), \quad r \geq r_0. \quad (4)$$

Here  $r_0$  is the radius of the fiber and it is much smaller than the capillary length  $r_c$ ; the height  $h(t)$  and the dynamic contact angle  $\theta(t)$  are two parameters to characterize the evolution of

the interface. The function (4) is a solution of the Young-Laplace equation for the liquid-air meniscus near a thin cylinder[3]. The assumption of the profile actually implies that the liquid-air interface is in local equilibrium away from the contact line. This is a good approximation when the velocity of the fiber is relatively small, i.e. the capillary number is small in the system [40, 53].

Since the gravity will prevent the meniscus from extending indefinitely, we can assume the lateral dimension of the meniscus does not exceed the capillary length  $r_c$ . Suppose the flat part of the liquid-air interface is given by  $z = 0$ , then we have  $H(r_c) = 0$ . This leads to

$$h(t) = r_0 \cos \theta(t) \ln \left( \frac{r_c + \sqrt{r_c^2 - r_0^2 \cos^2 \theta(t)}}{r_0 \cos \theta(t)} \right). \quad (5)$$

It gives a restriction condition between  $h(t)$  and  $\theta(t)$ . In other words, the two parameters are not independent. We can choose  $\theta(t)$  as the only slow parameter to characterize the evolution of the system. The evolving equation of  $\theta(t)$  will be derived by using the Onsager principle.

### A. The surface energy

We first calculate the potential energy in the system. Since the length of the meniscus is smaller than the capillary length, the gravitational energy can be ignored. The total potential energy  $A$  is composed of some surface energies:

$$A = A_{liquid} + A_{fiber}, \quad (6)$$

where  $A_{liquid}$  and  $A_{fiber}$  are the energy of the liquid-air interface and that of the fiber surface, respectively.

Let  $L$  be the total length of the fiber and  $L_0(t)$  be the length of the fiber under the horizontal surface  $z = 0$  at time  $t$ . Notice that the position of the contact line is given by

$$\tilde{h} = h - r_0 \cos \theta \ln \left( \frac{1 + \sin \theta}{\cos \theta} \right) \approx r_0 \cos \theta \ln \left( \frac{2r_c}{r_0(1 + \sin \theta)} \right). \quad (7)$$

In the approximation, we have used (5) and the assumption  $r_0 \ll r_c$ . Then we have

$$A_{fiber} = -2\pi\gamma r_0 \int_{-L_0(t)}^{\tilde{h}} \cos \theta_Y(z, t) dz. \quad (8)$$

The Young's angle  $\theta_Y(z, t)$  depends on  $z$  and  $t$  since the fiber surface is chemically inhomogeneous and it is moving relative to the horizontal surface  $z = 0$ . In addition, since the fiber moves with a velocity  $v$ , we can assume  $\theta_Y(z) = \tilde{\theta}_Y(z - vt)$  for a given function  $\tilde{\theta}_Y$ , which describes the distribution of the chemical inhomogeneity on the fiber.

The surface energy  $A_{liquid}$  is given by

$$A_{liquid} = 2\pi\gamma \int_{r_0}^{r_c} \sqrt{1 + (\partial_r H)^2} r dr. \quad (9)$$

Direct calculations give

$$A_{liquid} = \pi\gamma \left[ r_c \sqrt{r_c^2 - r_0^2 \cos^2 \theta} - r_0^2 \sin \theta + r_0^2 \cos^2 \theta \ln \left( \frac{r_c + \sqrt{r_c^2 - r_0^2 \cos^2 \theta}}{r_0(1 + \sin \theta)} \right) \right]. \quad (10)$$

To use the Onsager principle, we need compute the derivative of the total energy with respect to  $\theta$ . From (8), it is easy to compute

$$\frac{dA_{fiber}}{d\theta} = \frac{dA_{fiber}}{d\tilde{h}} \frac{d\tilde{h}}{d\theta} = -2\pi\gamma r_0^2 \cos \tilde{\theta}_Y(\tilde{h} - vt) g(\theta), \quad (11)$$

with

$$g(\theta) = r_0^{-1} \frac{d\tilde{h}}{d\theta} \approx - \left[ \sin \theta \ln \left( \frac{2r_c}{r_0(1 + \cos \theta)} \right) + 1 - \sin \theta \right]. \quad (12)$$

By direct calculations from (10), we obtain

$$\begin{aligned} \frac{dA_{liquid}}{d\theta} &= \pi\gamma r_0^2 \left[ \frac{r_c \cos \theta \sin \theta}{\sqrt{r_c^2 - r_0^2 \cos^2 \theta}} - \cos \theta - 2 \sin \theta \cos \theta \ln \left( \frac{r_c + \sqrt{r_c^2 - r_0^2 \cos^2 \theta}}{r_0(1 + \sin \theta)} \right) \right. \\ &\quad \left. + \frac{\cos^2 \theta}{r_c + \sqrt{r_c^2 - r_0^2 \cos^2 \theta}} \cdot \frac{r_0^2 \sin \theta \cos \theta}{\sqrt{r_c^2 - r_0^2 \cos^2 \theta}} - \frac{\cos^3 \theta}{1 + \sin \theta} \right] \\ &\approx \pi\gamma r_0^2 \cos \theta \left[ \sin \theta - 1 - 2 \sin \theta \ln \left( \frac{2r_c}{r_0(1 + \sin \theta)} \right) + \frac{r_0^2}{2r_c^2} \cos^2 \theta \sin \theta - \frac{\cos^2 \theta}{1 + \sin \theta} \right] \\ &\approx 2\pi\gamma r_0^2 \cos \theta g(\theta). \end{aligned}$$

Here we use  $r_0 \ll r_c$  in the above approximations. Combining the above analysis, we obtain

$$\frac{dA}{d\theta} = \frac{dA_{liquid}}{d\theta} + \frac{dA_{fiber}}{d\theta} \approx 2\pi\gamma r_0^2 g(\theta) [\cos \theta - \cos \tilde{\theta}_Y(\tilde{h} - vt)]. \quad (13)$$

This is a general force which makes the dynamic contact angle  $\theta$  to relax to its equilibrium value (the Young's angle).

## B. The energy dissipation

We then compute the viscous energy dissipations in the system. Since the capillary number is small, we can assume the viscous dissipations near the contact line is dominant in the system[3]. When the contact angle  $\theta$  is small, the Rayleigh dissipation function is approximately given by [3]

$$\Phi = \frac{3\pi\eta r_0}{\theta} |\ln \varepsilon| U^2, \quad (14)$$

where  $U$  is the slip velocity of the contact line on the fiber and  $\varepsilon$  is a cut-off parameter to avoid the singular integration. The formula (14) can be derived by computing the viscous energy dissipation in a two dimensional wedge region as shown in Figure 2 by lubrication approximations. It works only when  $\theta \ll 1$ .

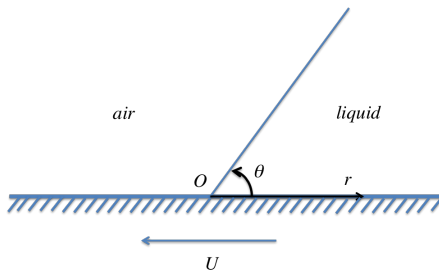


FIG. 2. Fluid near a contact line

When the contact angle  $\theta$  is large, we need an alternative calculations for the viscous dissipations. Here we adopt the method in [22]. We first compute the dissipation in the two-dimensional wedge region. As shown in Figure 2, we choose a polar coordinate system. The origin  $O$  is set at the contact point. The liquid region is given by  $\{(r, \phi) | r > 0, 0 < \phi < \theta\}$ . Suppose the solid surface moves with a velocity  $U$ . The velocity field of the liquid is described by the Stokes equation. By the incompressibility condition, we can define a stream function

$$\psi(r, \phi) = r(a \sin \phi + b \cos \phi + c\phi \sin \phi + d\phi \cos \phi), \quad (15)$$

where  $a, b, c$  and  $d$  are parameters to be determined. Then the velocities in the radial and angular directions are given by

$$v_r = -\frac{1}{r} \partial_\phi \psi, \quad v_\phi = \partial_r \psi. \quad (16)$$



The boundary conditions of the fluid equation are

$$\begin{cases} \partial_r \psi = 0 & \text{on } \phi = 0 \text{ and } \phi = \theta, r > 0, \\ -\frac{1}{r} \partial_\phi \psi = U & \text{on } \phi = 0, r > 0, \\ \partial_{\phi\phi} \psi = 0 & \text{on } \phi = \theta, r > 0. \end{cases} \quad (17)$$

Here we adopt a no-slip boundary condition on the solid surface and set the normal velocity and the tangential stress to be zero on the liquid-air interface. By substituting the equation (15) to the boundary conditions (17), we obtain

$$a = -\frac{\theta U}{\theta - \sin \theta \cos \theta}, \quad b = 0, \quad c = \frac{\sin^2 \theta U}{\theta - \sin \theta \cos \theta}, \quad d = \frac{\sin \theta \cos \theta U}{\theta - \sin \theta \cos \theta} \quad (18)$$

Then the equation (16) leads to

$$\begin{cases} v_r = -[(a + d) \cos \phi + c \sin \phi + c\phi \cos \phi - d\phi \sin \phi], \\ v_\phi = a \sin \phi + c\phi \sin \phi + d\phi \cos \phi, \end{cases} \quad (19)$$

where  $a, c, d$  are given in (18). Let  $\mathbf{r}$  and  $\mathbf{n}$  be the unit vectors along the radial and angular directions, respectively. Direct computations yield

$$\nabla \mathbf{v} = \frac{2}{r} (d \sin \phi - c \cos \phi) \mathbf{n} \mathbf{r}^T.$$

Then the total viscous energy dissipation in the two dimensional wedge (liquid) region can be computed out as

$$\Psi = \int \int \eta |\nabla \mathbf{v}|^2 r d\phi dr = \frac{2\eta |\ln \varepsilon| \sin^2 \theta U^2}{\theta - \sin \theta \cos \theta},$$

where  $\varepsilon$  is the cut-off parameter.

Using the above analysis result, the energy dissipation in our system can be approximated by  $4\pi r_0 \Psi$ . Then the Rayleigh dissipation function  $\Phi$ , which is defined as half of the total energy dissipation, is given by

$$\Phi = 2\pi \eta r_0 |\ln \varepsilon| \frac{\sin^2 \theta}{\theta - \sin \theta \cos \theta} U^2. \quad (20)$$

The formula is consistent with the equation (14) when the contact angle is small. Actually, when  $\theta \ll 1$ ,  $\sin \theta \sim \theta - \frac{\theta^3}{6} + \dots$ ,  $\cos \theta = 1 - \frac{\theta^2}{2} + \dots$ , we easily have  $\frac{\sin^2 \theta}{\theta - \sin \theta \cos \theta} \sim \frac{3}{2\theta}$ . The equation (20) will reduce to (14).

In Equation (20),  $U$  is the relative velocity of between the fiber and the contact line. In our case, it is written as

$$U = \dot{\tilde{h}} - v = \frac{d\tilde{h}}{d\theta}\dot{\theta} - v = r_0g(\theta)\dot{\theta} - v,$$

where we have used (12). Then the Rayleigh dissipation function is

$$\Phi = \frac{2\pi\eta r_0 |\ln \varepsilon| \sin^2 \theta}{\theta - \sin \theta \cos \theta} (r_0g(\theta)\dot{\theta} - v)^2. \quad (21)$$

We can further compute

$$\frac{d\Phi}{d\dot{\theta}} = \frac{4\pi\eta r_0^2 |\ln \varepsilon| \sin^2 \theta}{\theta - \sin \theta \cos \theta} g(\theta) (r_0g(\theta)\dot{\theta} - v). \quad (22)$$

### C. The evolution equation for the dynamic contact angle

By using the Onsager principle for the dynamic contact angle, we have  $\frac{\partial \Phi}{\partial \dot{\theta}} + \frac{\partial A}{\partial \theta} = 0$ . Combining with the previous analytic results, we obtain a dynamic equation for the contact angle  $\theta$ ,

$$\frac{2\eta |\ln \varepsilon| \sin^2 \theta}{\theta - \sin \theta \cos \theta} (r_0g(\theta)\dot{\theta} - v) + \gamma [\cos \theta - \cos \tilde{\theta}_Y(\tilde{h} - vt)] = 0. \quad (23)$$

Introduce a notation

$$f(\theta) = \frac{\theta - \sin \theta \cos \theta}{2 |\ln \varepsilon| \sin^2 \theta}. \quad (24)$$

The equation (23) is simplified to

$$\dot{\theta} = (r_0g(\theta))^{-1} [v - v^* f(\theta) (\cos \theta - \cos \tilde{\theta}_Y(\tilde{h} - vt))]. \quad (25)$$

where  $v^* = \frac{\gamma}{\eta}$  and  $\tilde{h}$  is given in (7). This is an ordinary differential equation for  $\theta$  and can be solved easily by standard numerical methods.

For convenience in applications, we can rewrite (25) into a different equivalent form. Introduce a new variable  $Z = \tilde{h} - vt$ , which represents the position of the contact line relative to the fiber surface. By (12) and (25), we can compute

$$\frac{dZ}{dt} = \frac{d\tilde{h}}{d\theta}\dot{\theta} - v = r_0g(\theta)\dot{\theta} - v = -v^* f(\theta) [\cos \theta - \cos \tilde{\theta}_Y(Z)].$$

The equation (25) is equivalent to an ordinary differential system for  $\theta$  and  $Z$ :

$$\begin{cases} \dot{\theta} = (r_0g(\theta))^{-1} [v^* f(\theta) (\cos \tilde{\theta}_Y(Z) - \cos \theta) + v], \\ \dot{Z} = v^* f(\theta) (\cos \tilde{\theta}_Y(Z) - \cos \theta), \end{cases} \quad (26)$$

where the dimensionless notations  $f(\theta)$  and  $g(\theta)$  are given in (24) and (12), respectively. The structure of the system (26) is similar to a model derived from the analysis of the phase-field equation in [47], where the viscous dissipation is ignored.

#### D. Discussions

In general the ODE system (26) can not be solved explicitly. But we can do some simple analysis to give some physical understandings for the equation. We first consider the case when the fiber surface is homogeneous. We can assume  $\tilde{\theta}_Y \equiv \theta_0$  for a constant  $\theta_0$ . Then the two equation in (26) are decoupled. The evolution of the dynamic contact angle  $\theta$  can be determined solely by the first equation. It is easy to see that there exists a steady state, in which the contact angle does not change with time, when

$$v = v^* f(\theta)(\cos \theta - \cos \theta_0). \quad (27)$$

The equation gives a relation between the capillary number  $Ca = v/v^*$  and the dynamic contact angle  $\theta$ . It can be rewritten as

$$\theta = G(\theta_0, Ca), \quad (28)$$

where  $G$  is an implicit function. This implies that the dynamic contact angle in steady state is determined the Young's angle and the capillary number. By solving the nonlinear algebraic equation (27) numerically, we draw a curve for  $\theta = G(\theta_0, Ca)$  for  $\theta_0$  in Figure 3. The curve shows that the dynamic contact angle in steady state is a monotone function with respect to  $Ca$ . The equilibrium contact angle is equal to the Young's angle  $\theta_0$  when  $Ca = 0$ . When  $Ca > 0$ (the fiber moves up), the dynamic contact angle corresponds to a receding angle such that  $\theta < \theta_0$ . When  $Ca < 0$ (the fiber moves down),  $\theta$  corresponds to an advancing contact angle which is larger than  $\theta_0$ . The results are consistent with those in previous analysis [3, 23, 38].

When the fiber surface is chemically inhomogeneous, it is more difficult to analyze for the equation (26). We consider a special case where the surface is composed by two materials with different Young's angles  $\theta_{Y1}$  and  $\theta_{Y2}$  (suppose  $\theta_{Y1} > \theta_{Y2}$ ). The two materials are distributed periodically on the surface. If the period is large, the motion of the contact line on one material is like that on a homogeneous surface. The dynamic contact angle may

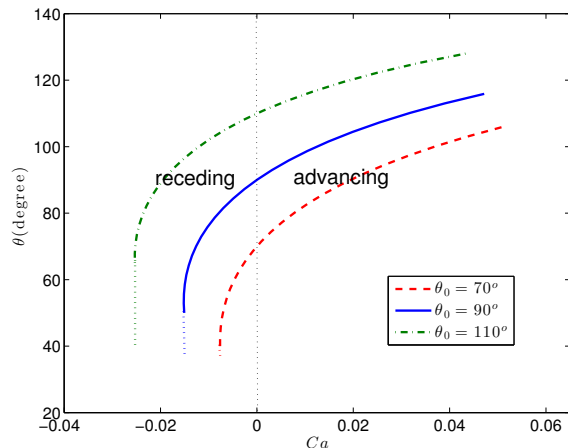


FIG. 3. The relation between the dynamic contact angle and the Capillary number in steady state.

alternate between two different steady states. The corresponding dynamic contact angles are  $\theta_1 = G(\theta_{Y1}, Ca)$  and  $\theta_2 = G(\theta_{Y2}, Ca)$ , respectively. Since  $\theta_{Y1} > \theta_{Y2}$ ,  $\theta_1$  gives an upper bound for the contact angle while  $\theta_2$  gives a lower bound. In the next section, we will verify this numerically. When  $Ca$  goes to zero,  $\theta_1$  and  $\theta_2$  will converge to  $\theta_{Y1}$  and  $\theta_{Y2}$ , respectively. This is consistent with the previous analysis for the quasi-static CAH in [13, 14].

#### IV. NUMERICAL RESULTS

We show some numerical results for the equation (26) for some chemically inhomogeneous fiber surfaces. We assume that  $\tilde{\theta}_Y(z)$  is a period function with a period  $l$  such that  $\delta = l/r_c \ll 1$ . Then we can write  $\tilde{\theta}_Y(z) = \vartheta_Y(\frac{z}{l})$ , with a function  $\vartheta_Y(\cdot)$  being a function with period 1.

We non-dimensionalize the equation (26). Suppose the characteristic velocity is given by the velocity  $v^* = \frac{\gamma}{\eta}$  and the characteristic length scale is the capillary length  $r_c$ . Then the characteristic time is given by  $t_c = r_c/v^*$ . Introduce some dimensionless parameters  $\delta_0 = \frac{r_0}{r_c}$  and  $Ca = \frac{v}{v^*}$ , and use  $\tilde{Z}$  to represent the dimensionless coordinate  $\frac{Z}{r_c}$ , then the system (26) could be rewritten as

$$\begin{cases} \dot{\theta} = (\delta_0 g(\theta))^{-1} \left[ f(\theta)(\cos \vartheta_Y(\frac{\tilde{Z}}{\delta}) - \cos \theta) + Ca \right], \\ \dot{\tilde{Z}} = f(\theta)(\cos \vartheta_Y(\frac{\tilde{Z}}{\delta}) - \cos \theta). \end{cases} \quad (29)$$

Here the function  $f(\theta)$  is given in (24) and  $g(\theta)$  can be rewritten as

$$g(\theta) = -\sin \theta \ln \left( \frac{2\delta_0^{-1}}{1 + \sin \theta} \right) + \sin \theta - 1.$$

For simplicity in notations, we still use  $Z$  to represent the dimensionless  $\tilde{Z}$  hereinafter.

The equation (29) can be solved easily by the standard Runge-Kutta method. We set  $\delta_0 = 4.03 \times 10^{-4}$  which is chosen from [20]. The cut-off parameter is chosen to satisfy  $\ln \varepsilon = 13.8$ , which is a typical value used in literature[3]. In the following, we show some numerical results for some special choices of  $\vartheta_Y(z)$ .

In the first example, we choose  $\tilde{\theta}_Y(z) = 110^\circ + 8^\circ \cdot \sin(2\pi z/\delta)$ . This is a smooth periodic function. The maximal Young's angle is  $\theta_{Ymax} = 118^\circ$  and minimal Young's angle is  $\theta_{Ymin} = 102^\circ$ .

We first set  $|Ca| = 0.0001$  and test for different period  $\delta$ . In this case, the capillary number is very small so that it is very close to a quasi-static process. Some typical numerical results are shown in the first two subfigures of Figure 4. They are the trajectories of the solution of (29) in the phase space. Both the dynamic contact angle and receding contact angles are shown with respect to  $Z$ . When the oscillation of the Young's angle  $\tilde{\theta}_Y$  is weak ( $\delta = 0.003$ ), the advancing and receding cases have almost the same trajectory in the phase space. There seems no hysteresis. When  $\delta$  decreases, the stronger oscillation of  $\tilde{\theta}_Y$  corresponds to stronger chemical inhomogeneity. Then the advancing and receding processes may follow different trajectories. When  $\delta = 0.0003$ , there is obvious CAH phenomenon. The advancing and receding contact angles oscillate around different values. The largest dynamic contact angle is about  $118.02^\circ \approx G(\theta_{Ymax}, -|Ca|)$  and the smallest contact angel is about  $101.9^\circ \approx G(\theta_{Ymin}, |Ca|)$ . Here  $G$  is an implicit function given in (28). Since the capillary number is very small, the two angles are very close to the largest Young's and smallest Young's angles in the system.

We then set  $|Ca| = 0.0025$  and test for different  $\delta$ . Some typical numerical results are shown in the last two subfigures of Figure 4. We can see that when the inhomogeneity is relatively weak ( $\delta = 0.003$ ), the advancing and receding processes follow different but partially overlapped trajectories. The largest advancing contact angle is about  $119.33^\circ \approx G(\theta_{Ymax}, -|Ca|)$  and the smallest receding contact angle is about  $99.12^\circ \approx G(\theta_{Ymin}, |Ca|)$ . When the chemical inhomogeneity becomes strong enough (e.g.  $\delta = 0.0003$ ), the trajectories separate completely for the advancing and receding cases. This corresponds to obvious CAH.

The largest advancing contact angle is slightly smaller than the upper bound  $119.33^\circ$  and the advancing contact angle is slightly larger than the lower bound  $99.12^\circ$ . This is because the strong inhomogeneity and the large velocity of the fiber make the motion of the contact angle away from a steady state.

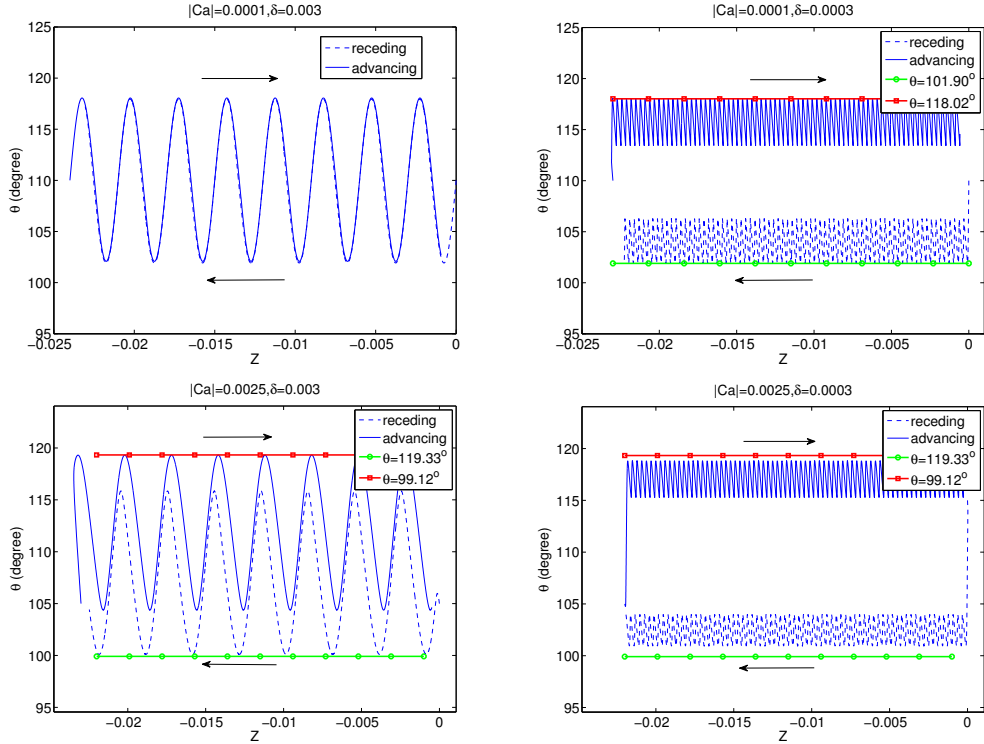


FIG. 4. Trajectories of the dynamic contact angles and the contact line positions in phase plane for different  $\delta$  and  $Ca$ . (Example 1)

In the second example, we set  $\tilde{\theta}_Y(z) = 100^\circ + 20^\circ \cdot \tanh(10 \sin(2\pi z/\delta))$ . This approximates a chemically patterned surface with different Young's angles  $\theta_A = 120^\circ$  and  $\theta_B = 80^\circ$ .

We first set  $|Ca| = 0.0001$  and test for different  $\delta$ . Some typical numerical results are shown in the first two subfigures in Figure 5. We see that the advancing and receding trajectories do not coincide even for very large period  $\delta$  (e.g  $\delta = 0.03$ ). This is different from the case when  $\theta_Y$  is a smooth function as in the first example. The phenomena are like that the pinning of the contact line by a single defect in quasi-static processes[5, 8]. When  $\delta$  becomes small enough, the two trajectories separate completely. When  $\delta = 0.0003$ , the advancing and receding contact angles oscillate around different values. The largest contact angle is almost equal to the upper bound  $120.00^\circ \approx G(\theta_A, -|Ca|)$  and the smallest contact

angle is almost equal to the lower one  $79.83^\circ \approx G(\theta_B, |Ca|)$ . Since  $|Ca|$  is small, the two values are close to the two Young's angles. The results are consistent to the previous analysis for the quasi-static CAH on chemically patterned surface[13, 14].

We then set  $|Ca| = 0.0025$  and test for different periods  $\delta$ . Some typical numerical results are shown in the last two subfigures in Figure 5. We can observe clear stick-slip behaviour for  $\delta = 0.003$ . The stick behaviour corresponds to the case that the position of the contact line does not change much while the contact angle change dramatically. The slip behaviour corresponds to a process that both the contact line and the contact angle change dramatically(the slope parts on the trajectories). The advancing and receding processes have different but slightly overlapped trajectories. The largest advancing angle almost equal to the upper bound  $121.29^\circ = G(\theta_A, -|Ca|)$  and the smaller receding angle is almost the lower bound  $76.52^\circ = G(\theta_B, |Ca|)$ . When the contact angles reaches the upper and lower bounds, there exist some steady states that the contact angles does not change while the contact line moves. When  $\delta = 0.0003$ , the advancing and receding trajectories separate completely. The advancing contact angle is slightly smaller than the upper bound ( $121.29^\circ$ ) and the receding contact angle is slightly larger than the lower one ( $76.52^\circ$ ). This is because there is no steady state in the advancing or receding processes. However, the deviation is smaller than that in the previous example(comparing with the last two subfigures in Figure 4).

In the last example, we investigate in more details on how the dynamic CAH be affected the fiber velocity. We choose  $\tilde{\theta}_Y$  as that in the first example, which is a smooth function. We do numerical simulations for various capillary numbers  $|Ca| = 0.0025, 0.05, 0.01$  and  $0.02$ . Some numerical results are shown in Figure 6. The first subfigure corresponds to the case  $\delta = 0.0003$  and the second is for the case  $\delta = 0.00003$ . Similar to that in Figure 4, we could see clearly the CAH in all these cases. We could also see that the advancing contact angle increases and the receding contact angle decreases when the absolute value of the capillary number increases(i.e. when the fiber velocity increases). More interesting, the dependence of the advancing and receding contact angles on the velocity are asymmetric in the sense that the receding angle changes more dramatically than the advancing angle. This can be explained by the behaviour of  $G(\theta, \cdot)$  as shown in Figure 3. the slope of the curve in the receding part is larger than that in the advancing part. This implies that the receding angle will change more dramatically than the advancing angle. The asymmetric dependence of the CAH on the velocity is consistent with that observed in physical experiments. The third

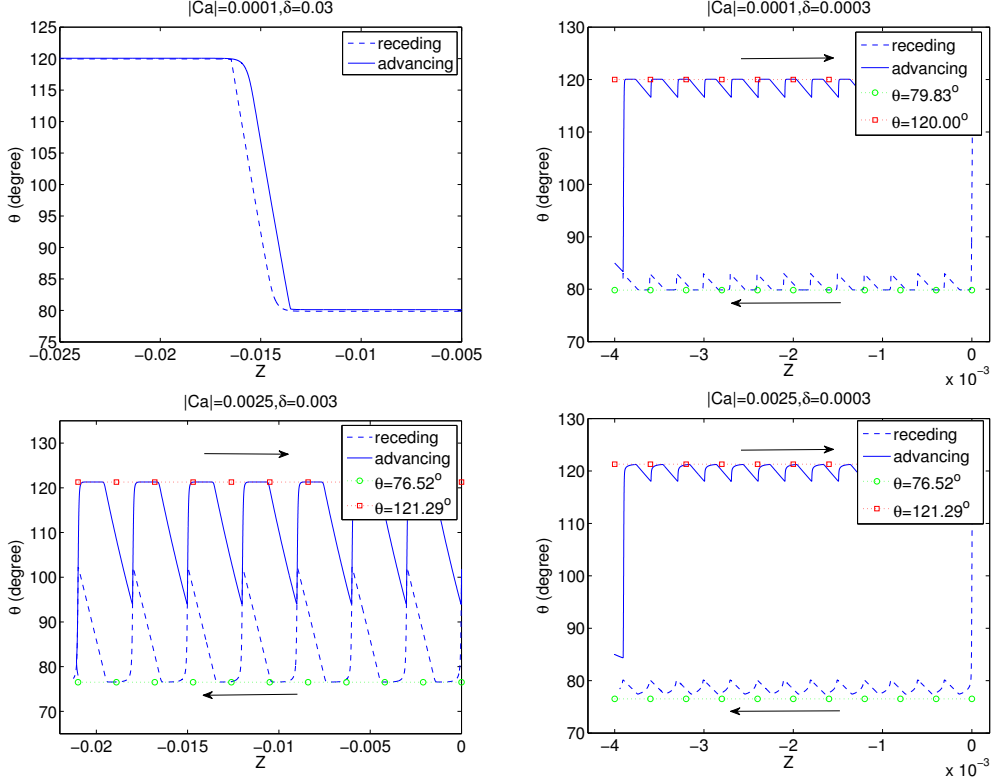


FIG. 5. Trajectories of the dynamic contact angles and the contact line positions in phase plane for different  $\delta$  and  $Ca$ . (Example 2)

subfigure in Figure 6, which is taken from [20], shows the velocity dependence of CAH in experiments. We can see that the behaviour of the dynamic CAH is very like that in our numerical simulations. Finally, we would like to remark that similar phenomenon has been observed in a pure phase-field model[48], without considering the viscous dissipation in fluid. The numerical results by the reduced model (29) are more consistent with the experiments quantitatively, since viscous dissipations are correctly included by the Onsager principle.

## V. CONCLUSIONS

We develop a simple model for dynamic CAH on a fiber with chemically inhomogeneous surface by using the Onsager principle as an approximation tool. The model is an ordinary differential system for the apparent contact angle and the contact line. It is easy to analyse and to solve numerically. The analytical and numerical results show that the model captures the essential phenomena of the CAH. By using the model, we derive an upper bound for



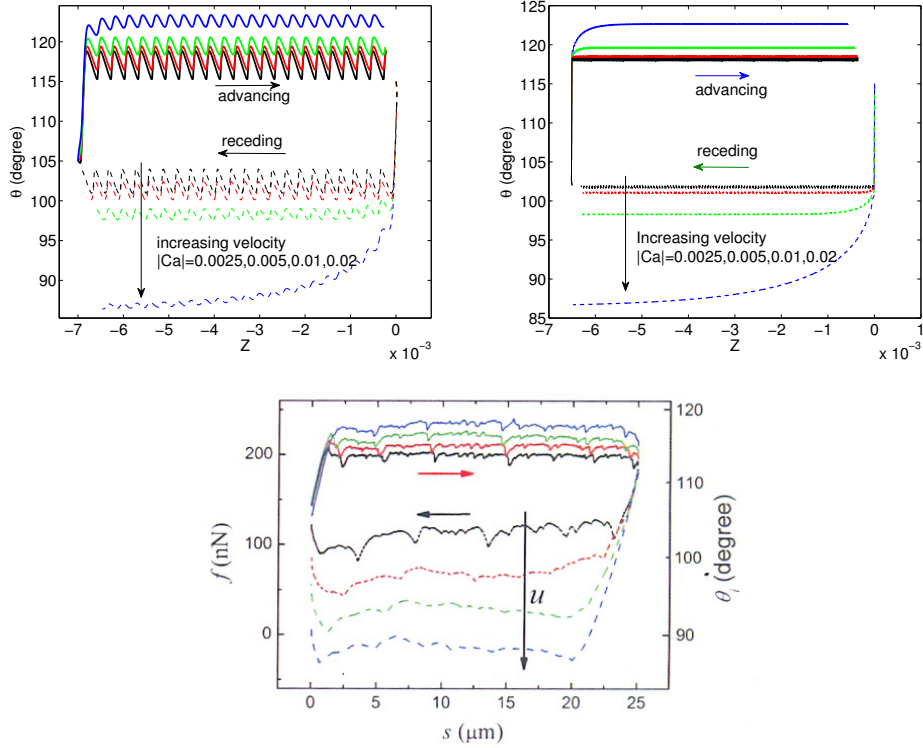


FIG. 6. Asymmetry dependence of the advancing and receding contact angles on the wall velocity. The last subfigure shows the experimental results in [20]

the dynamic advancing contact angle and a lower bound for the receding angle. The model is able to characterize the asymmetric dependence of the advancing and receding contact angles on the fiber velocity, which has been observed in recent experiments.

Finally, we would like to remark that the real solid surface in experiments is more complicated than the setup in this paper. The chemical inhomogeneity or geometrical roughness of the solid surface may be random and the distribution of defects may lead to very complicated contact line motion. For example, many sophisticated phenomena have been observed in [54]. In addition, the heat noise may also affect the relaxation behaviour of the contact line when the radius of the fiber is in micro-scale. These effects will be studied in future study.

### Acknowledgments:

The author would like to thank Professor Masao Doi, Tiezheng Qian, and Penger Tong for their helpful discussions. This work was supported in part by NSFC grants DMS-11971469

and the National Key R&D Program of China under Grant 2018YFB0704304 and Grant 2018YFB0704300.

---

- [1] T. Young, “An essay on the cohesion of fluids,” *Philos. Trans. R. Soc. London* **95**, 65–87 (1805).
- [2] P.G. de Gennes, “Wetting: Statics and dynamics,” *Rev. Mod. Phys.* **57**, 827–863 (1985).
- [3] P.G. de Gennes, F. Brochard-Wyart, and D. Quere, *Capillarity and Wetting Phenomena* (Springer Berlin, 2003).
- [4] D. Bonn, J. Eggers, J. Indekeu, J. Meunier, and E. Rolley, “Wetting and spreading,” *Rev. Mod. Phys.* **81**, 739–805 (2009).
- [5] M. Delmas, M. Monthieux, and T. Ondarçuhu, “Contact angle hysteresis at the nanometer scale,” *Phys. Rev. Lett.* **106**, 136102 (2011).
- [6] A. Giacomello, L. Schimmele, and S. Dietrich, “Wetting hysteresis induced by nanodefects,” *Proc. Nat. Acad. Sci.* **113**, E262–E271 (2016).
- [7] R. E. Johnson Jr. and R. H. Dettre, “Contact angle hysteresis. iii. study of an idealized heterogeneous surfaces,” *J. Phys. Chem.* **68**, 1744–1750 (1964).
- [8] J. F. Joanny and P.-G. De Gennes, “A model for contact angle hysteresis,” *J. Chem. Phys.* **81**, 552–562 (1984).
- [9] L. W. Schwartz and S. Garoff, “Contact angle hysteresis on heterogeneous surfaces,” *Langmuir* **1**, 219–230 (1985).
- [10] C. W. Extrand, “Model for contact angles and hysteresis on rough and ultraphobic surfaces,” *Langmuir* **18**, 7991–7999 (2002).
- [11] G. Whyman, E. Bormashenko, and T. Stein, “The rigorous derivative of young, cassie-baxter and wenzel equations and the analysis of the contact angle hysteresis phenomenon,” *Chem. Phy. Letters* **450**, 355–359 (2008).
- [12] A. Turco, F. Alouges, and A. DeSimone, “Wetting on rough surfaces and contact angle hysteresis: numerical experiments based on a phase field model,” *ESAIM: Math. Mod. Numer. Anal.* **43**, 1027–1044 (2009).
- [13] X. Xu and X. P. Wang, “Analysis of wetting and contact angle hysteresis on chemically patterned surfaces,” *SIAM J. Appl. Math.* **71**, 1753–1779 (2011).

- [14] M. Hatipogullari, C. Wylock, M. Pradas, S. Kalliadasis, and P. Colinet, “Contact angle hysteresis in a microchannel: Statics,” *Phys. Rev. Fluids* **4**, 044008 (2019).
- [15] W. Choi, A. Tuteja, J. M. Mabry, R. E. Cohen, and G. H. McKinley, “A modified cassiebaxter relationship to explain contact angle hysteresis and anisotropy on non-wetting textured surfaces,” *J. Colloid Interface Sci.* **339**, 208–216 (2009).
- [16] R. Raj, R. Enright, Y. Zhu, S. Adera, and E. N. Wang, “Unified model for contact angle hysteresis on heterogeneous and superhydrophobic surfaces,” *Langmuir* **28**, 15777–15788 (2012).
- [17] X. Xu and X. P. Wang, “The modified cassie’s equation and contact angle hysteresis,” *Colloid Polym. Sci.* **291**, 299–306 (2013).
- [18] X. Xu, “Modified wenzel and cassie equations for wetting on rough surfaces,” *SIAM J. Appl. Math.* **76**, 2353–2374 (2016).
- [19] C. Priest, R. Sedev, and J. Ralston, “A quantitative experimental study of wetting hysteresis on discrete and continuous chemical heterogeneities,” *Colloid Polym. Sci.* **291**, 271–277 (2013).
- [20] D. Guan, Y. Wang, E. Charlaix, and P. Tong, “Asymmetric and speed-dependent capillary force hysteresis and relaxation of a suddenly stopped moving contact line,” *Phys. Rev. Lett.* **116**, 066102 (2016).
- [21] P. Collet, J. De Coninck, F. Dunlop, and A. Regnard, “Dynamics of the contact line: Contact angle hysteresis,” *Phys. Rev. Lett.* **79**, 3704 (1997).
- [22] C. Huh and L.E. Scriven, “Hydrodynamic model of steady movement of a solid/liquid/fluid contact line,” *J. colloid Interface Sci.* **35**, 85–101 (1971).
- [23] R. Cox, “The dynamics of the spreading of liquids on a solid surface. Part 1. Viscous flow,” *J. Fluid Mech.* **168**, 169–194 (1986).
- [24] D. Jacqmin, “Contact-line dynamics of a diffuse fluid interface,” *J. Fluid Mech.* **402**, 57–88 (2000).
- [25] T. Qian, X.P. Wang, and P. Sheng, “Molecular scale contact line hydrodynamics of immiscible flows,” *Phys. Rev. E* **68**, 016306 (2003).
- [26] W. Ren and W. E, “Boundary conditions for the moving contact line problem,” *Phys. Fluids* **19**, 022101 (2007).
- [27] P. Yue, C. Zhou, and J. J. Feng, “Sharp-interface limit of the Cahn-Hilliard model for moving contact lines,” *J. Fluid Mech.* **645**, 279–294 (2010).

- [28] J. H. Snoeijer and B. Andreotti, “Moving contact lines: scales, regimes, and dynamical transitions,” *Annual Rev. Fluid Mech.* **45**, 269–292 (2013).
- [29] Y. Sui, H. Ding, and P. Spelt, “Numerical simulations of flows with moving contact lines,” *Annual Rev. Fluid Mech.* **46**, 97–119 (2014).
- [30] X. Xu, Y. Di, and H. Yu, “Sharp-interface limits of a phase-field model with a generalized navier slip boundary condition for moving contact lines,” *J. Fluid Mech.* **849**, 805–833 (2018).
- [31] X.P. Wang, T. Qian, and P. Sheng, “Moving contact line on chemically patterned surfaces,” *J. Fluid Mech.* **605**, 59–78 (2008).
- [32] W. Ren and W. E, “Contact line dynamics on heterogeneous surfaces,” *Phys. Fluids* **23**, 072103 (2011).
- [33] R. Golestanian, “Moving contact lines on heterogeneous substrates,” *Phil. Trans. Roy. Soc. London. A* **362**, 1613–1623 (2004).
- [34] L. Onsager, “Reciprocal relations in irreversible processes. i.” *Phys. Rev.* **37**, 405 (1931).
- [35] L. Onsager, “Reciprocal relations in irreversible processes. ii.” *Phys. Rev.* **38**, 2265 (1931).
- [36] M. Doi, “Onsager principle as a tool for approximation,” *Chinese Phys. B* **24**, 020505 (2015).
- [37] Y. Di, X. Xu, J. Zhou, and M. Doi, “Thin film dynamics in coating problems using onsager principle,” *Chinese Phys. B* **27**, 024501 (2018).
- [38] X. Xu, Y. Di, and M. Doi, “Variational method for contact line problems in sliding liquids,” *Phys. Fluids* **28**, 087101 (2016).
- [39] Y. Di, X. Xu, and M. Doi, “Theoretical analysis for meniscus rise of a liquid contained between a flexible film and a solid wall,” *Europhys. Lett.* **113**, 36001 (2016).
- [40] S. Guo, X. Xu, T. Qian, Y. Di, M. Doi, and P. Tong, “Onset of thin film meniscus along a fibre,” *J. Fluid Mech.* **865**, 650–680 (2019).
- [41] X. Man and M. Doi, “Ring to mountain transition in deposition pattern of drying droplets,” *Phys. Rev. Lett.* **116**, 066101 (2016).
- [42] W. Jiang, Q. Zhao, T. Qian, D. J. Srolovitz, and W. Bao, “Application of onsager’s variational principle to the dynamics of a solid toroidal island on a substrate,” *Acta Mater.* **163**, 154–160 (2019).
- [43] T. Yu, J. Zhou, and M. Doi, “Capillary imbibition in a square tube,” *Soft matter* **14**, 9263–9270 (2018).
- [44] J. Zhou and M. Doi, “Dynamics of viscoelastic filaments based on onsager principle,” *Phys.*

- Rev. Fluids **3**, 084004 (2018).
- [45] M. Doi, J. Zhou, Y. Di, and X. Xu, “Application of the onsager-machlup integral in solving dynamic equations in nonequilibrium systems,” Phys. Rev. E **99**, 063303 (2019).
- [46] T. Qian, X.P. Wang, and P. Sheng, “A variational approach to moving contact line hydrodynamics,” J. Fluid Mech. **564**, 333–360 (2006).
- [47] X.-P. Wang and X. Xu, “A dynamic theory for contact angle hysteresis on chemically rough boundary,” Discrete Contin. Dyn. Syst.(A) **37**, 1061–1073 (2017).
- [48] X. Xu, Y. Zhao, and X.-P. Wang, “Analysis for contact angle hysteresis on rough surfaces by a phase field model with a relaxed boundary condition,” SIAM J. Appl. Math. **79**, 2551–2568 (2019).
- [49] M. Doi, “Onsager’s variational principle in soft matter,” J. Phys. Cond Matt **23**, 284118 1–8 (2011).
- [50] M. Doi, *Soft Matter Physics* (Oxford University Press, 2013).
- [51] P.-G. De Gennes and J. Prost, *The physics of liquid crystals*, Vol. 83 (Oxford university press, 1993).
- [52] M. Doi, “Gel dynamics,” J. Phys. Soc. Japan **78**, 052001 (2009).
- [53] C.A. Fuentes, M. Hatipogullari, S. Van Hoof, Y. Vitry, S. Dehaeck, V. Du Bois, P. Lambert, P. Colinet, D. Seveno, and A.W. Van Vuure, “Contact line stick-slip motion and meniscus evolution on micrometer-size wavy fibres,” J. Colloid Interface Sci. **540**, 544–553 (2019).
- [54] D. Guan, Y. Wang, E. Charlaix, and P. Tong, “Simultaneous observation of asymmetric speed-dependent capillary force hysteresis and slow relaxation of a suddenly stopped moving contact line,” Phys. Rev. E **94**, 042802 (2016).